Brain source localization using a physics-driven structured cosparse representation of EEG signals

Laurent Albera, Srđan Kitić, Nancy Bertin, Gilles Puy, Rémi Gribonval

BRAIN SOURCE LOCALIZATION USING A PHYSICS-DRIVEN STRUCTURED COSPARSE REPRESENTATION OF EEG SIGNALS

L. Albera[(1,2,3)], *S. Kitić*[(3)], *N. Bertin*[(4)], *G. Puy*[(3)], *Rémi Gribonval*[(3)]

[(1)] Inserm, UMR 642, Rennes, F-35000, France   [(2)] LTSI, University of Rennes 1, Rennes, F-35000, France
[(3)] Inria, Centre Inria Rennes - Bretagne Atlantique, Rennes, F-35000, France
[(4)] IRISA, CNRS UMR 6074, Rennes, F-35000, France.

ABSTRACT

Localizing several potentially synchronous brain activities with low signal-to-noise ratio from ElectroEncephaloGraphic (EEG) recordings is a challenging problem. In this paper we propose a novel source localization method, named CoRE, which uses a Cosparse Representation of EEG signals. The underlying analysis operator is derived from physical laws satisfied by EEG signals, and more particularly from Poisson's equation. In addition, we show how physiological constraints on sources, leading to a given space support and fixed orientations for current dipoles, can be taken into account in the optimization scheme. Computer results, aiming at showing the feasability of the CoRE technique, illustrate its superiority in terms of estimation accuracy over dictionary-based sparse methods and subspace approaches.

Index Terms— Brain source localization, EEG, cosparsity, synchronous current activities.

1. INTRODUCTION

Electrical potentials produced by neuronal activity can be measured at the surface of the head using ElectroEncephaloGraphy (EEG). The sources of this neuronal activity (during either cognitive or pathological processes) can be localized provided that a model of sources and a model of volume conductor are defined. Most source localization algorithms use one of the two following source models: the point source model, which explains the data with a small number of equivalent current dipoles and the distributed source model, which uses thousands of dipoles. Whereas the latter allows for an estimation of the spatial extent of the source, it requires to make assumptions about the spatial source distribution, which may lead to blurred (or even distorted) solutions [1]. On the other hand, the former often gives helpful first approximations and superior performance in environments where there are few sources which are clustered [1]. Regarding head models,

they aim at representing geometrical and electrical properties of the different tissues composing the volume conductor. Various models were proposed going from concentric homogeneous spheres with isotropic conductivities to realistically shaped models with refined tissue conductivity values [2].

Numerous methods were developed to localize equivalent current dipoles from EEG recordings. Among them, beamforming techniques [3], subspace approaches such as MUSIC (MUltiple-SIgnal Classification) [4] and sparse methods [5] are the most popular. One can mention the RapMUSIC (Recursively applied MUSIC) [6] and FO-D-MUSIC (Fourth Order Deflationary MUSIC) [7] algorithms, which are sequential versions of MUSIC based on Second Order (SO) and Fourth Order (FO) statistics, respectively. Regarding the dictionary-based sparse techniques, the most famous is MCE (Minimum Current Estimate) [5], which computes minimum ℓ_1-norm estimates. Note that cosparse approaches were recently proposed applying for instance a discrete Gabor transform [8] as analysis operator [9] to the current source activities.

In this paper, we show how to derive an analysis operator derived from physical laws satisfied by EEG signals, and more particularly from Poisson's equation. As a result, we propose a new dipole localization method, named CoRE (physics-driven structured Cosparse Representation of EEG signals), taking into account physiological constraints on sources leading to a given space support and fixed orientations. Computer simulations demonstrate the feasability and the performance of the CoRE approach in comparison to the MCE technique especially for low Signal-to-Noise Ratio (SNR) values. We also illustrate the ability of CoRE in dealing with synchronous brain sources and overcoming the RapMUSIC and FO-D-MUSIC algorithms in such a practical context.

2. ASSUMPTIONS AND PROBLEM FORMULATION

It is commonly admitted that the electrical potential $v(\boldsymbol{r})$ recorded at location $\boldsymbol{r}$ of the head mostly reflects the activity of pyramidal cells located in the gray matter and oriented perpendicularly to the cortical surface. This activity is gen-

erally modeled by current dipoles. Given the geometry and the scalar field $\{\sigma(\boldsymbol{r})\}$ of electrical conductivities within the head, Poisson's equation [10] allows us to establish a link between the electrical potential $v(\boldsymbol{r})$ and the electrical activity of the current dipoles:

$$
\begin{aligned}
\operatorname{div}_{\boldsymbol{r}}(\sigma(\boldsymbol{r})\,\nabla_{\boldsymbol{r}}v(\boldsymbol{r})) = \\
\sum_{\boldsymbol{\rho}\in\mathcal{S}} s(\boldsymbol{\rho})(\delta(\boldsymbol{r}-\boldsymbol{\rho}^{-}) - \delta(\boldsymbol{r}-\boldsymbol{\rho}^{+}))/d
\end{aligned}
\tag{1}
$$

where $\boldsymbol{\rho}^{-}$ and $\boldsymbol{\rho}^{+}$ denote the positions of the two monopoles representing the current sink and source, respectively, d stands for the distance between the two monopoles, $s(\boldsymbol{\rho})$ is the electrical activity of the dipole located at position $\boldsymbol{\rho}$ and $\mathcal{S}$ denotes the gray matter. The location parameter $\boldsymbol{\rho}$ of the considered dipole is typically chosen half way between the two monopoles.

Let's consider the following assumptions:

A1. N potential values $v(\boldsymbol{r}_n)$ recorded at locations $\boldsymbol{r}_n$ of the scalp are available;

A2. Q current dipoles cover the gray matter $\mathcal{S}$;

A3. each current dipole is represented by two monopoles with opposite amplitudes;

A4. each current dipole is oriented orthogonally to the cortical surface;

A5. only P ($P \leq N$) current dipoles of $\mathcal{S}$ have a non-negligible amplitude.

Then, the brain source localization problem consists in identifying the locations $\boldsymbol{\rho}_p$ of the P dominant current dipoles belonging to $\mathcal{S}$ from the N-dimensional vector $\boldsymbol{x} = [v(\boldsymbol{r}_1),\dots,v(\boldsymbol{r}_N)]^{\mathsf{T}}$.

3. PHYSICS-DRIVEN STRUCTURED COSPARSE REPRESENTATION OF EEG SIGNALS

Now let's see how the brain source localization problem can be reformulated as a cosparse analysis model fitting problem based on a physics-driven structured cosparse representation of EEG signals.

3.1. Discretization of Poisson's equation

The CoRE approach described in section 4 requires an appropriate discretization of Poisson's equation in order to derive an equation of the form $\boldsymbol{\Omega}\,\boldsymbol{v} = \boldsymbol{z}$ from (1) where $\boldsymbol{\Omega}$ is a matrix denoting the so-called linear analysis operator [9] and where $\boldsymbol{z}$ is a sparse vector. The Finite Difference Method (FDM) and Finite Element Method (FEM) can be used to perform such a discretization. Note that these two methods allow us to take realistic head models into account such as those obtained from anatomical imaging modalities: Computed Tomography

(CT) and structural Magnetic Resonance Imaging (sMRI) for instance.

As an example, and without loss of generality, we consider the FDM in the following, and more particularly the FDM implemented by Witwer et al. [11] applying Kirchhoffs law at each node of the cubic grid. It is noteworthy that Witwer et al. gave an easy way of taking into account the skull-air boundary. The nodal points (voxels) exterior to the insulated boundary are assigned a conductivity that is so small that the flux leakage across the boundary can be made as small as desired. Another main advantage of Witwer's FDM is the way it is treating the internal boundaries and inhomogeneities, say by simply varying the conductivity values. Discretizing the volume as a $(L \times L \times L)$ uniform three-dimensional grid with spacing h, and applying Witwer's FDM to equation (1), we can express the total current flow value at a given voxel as a linear combination of the potentials measured in a close neighbourhood of this voxel (see equation (17) of appendix).

3.2. Toward a cosparse analysis model

The link between the total current flow value and the potentials derived from the discretization of Poisson's equation can be easily written in the matrix form $\boldsymbol{A}\,\boldsymbol{v} = \boldsymbol{i}$ where $\boldsymbol{v}$ and $\boldsymbol{i}$ are two vectors containing the potential and total current flow values, respectively, at the different nodes of the three-dimensional grid. The $(L^3 \times L^3)$ matrix $\boldsymbol{A}$ is symmetric, positive semidefinite, rank deficient by one and sparse with only seven non-zero components in each row [10]. Generally, instead of considering the singular linear system $\boldsymbol{A}\,\boldsymbol{v} = \boldsymbol{i}$, another possibility is to transform it into a regular one and solve this instead. The regular system is chosen such that its unique solution belongs to the set of solutions of the original singular system. As described in [10], the easiest approach is to fix the value of the potential to zero in one voxel. The special structure of the matrix $\boldsymbol{A}$ then allows us to cancel the corresponding row and column in $\boldsymbol{A}$ and also the respective entry in the right-hand side vector $\boldsymbol{i}$. This leads to a system for which the $(L^3 - 1 \times L^3 - 1)$ resulting matrix is symmetric and positive definite. By slight abuse of notation we continue to name this matrix $\boldsymbol{A}$. The solution of this system obviously solves the initial system with a zero potential value in the respective voxel.

Let ℓ^{-} and ℓ^{+} index the elements of $\boldsymbol{i}$ giving the amplitude of the monopoles located at positions $\boldsymbol{\rho}^{-}$ and $\boldsymbol{\rho}^{+}$, respectively, of the grid. According to assumptions (**A2**), (**A3**) and (**A4**), and knowing the geometry of the cortex, it is possible to build a set of Q different couples (ℓ_q^{-}, ℓ_q^{+}) indexing the Q dipoles of $\mathcal{S}$. Indeed, by covering the surface of the cortex with Q monopoles indexed by the integers ℓ_q^{-}, we can deduce the Q corresponding integers ℓ_q^{+} using (**A4**). We can thus factorize vector $\boldsymbol{i}$ as $\boldsymbol{i} = \boldsymbol{B}\,\boldsymbol{z}$ where $\boldsymbol{B} = (B_{\ell_1,\ell_2})$ is a

$(L^3 - 1 \times L^3 - 1)$ sparse matrix defined by:

$$B_{\ell_1,\ell_2} = \begin{cases} 1 & \text{if} \quad \ell_1 = \ell_2 \\ -1 & \text{if} \quad \ell_1 = \ell_q^+ \quad \text{and} \quad \ell_2 = \ell_q^- \\ 0 & \text{otherwise} \end{cases} \quad (2)$$

and where z is a $(L^3 - 1)$-dimensional P-sparse vector with $L^3 - 1 - Q$ known zero elements: the ℓ-th element of z is zero if $\ell \neq \ell_q^-$ for $q \in \{1, \ldots, Q\}$. Consequently, matrix B conveys our knowledge about the orientation of the Q dipoles of $\mathcal{S}$ and the amplitude of the monopoles associated with these dipoles. It is also an invertible matrix, since it is possible to permute its rows and columns such that a lower triangular matrix with ones on the diagonal is obtained. Regarding vector z, its non-zero elements represent the amplitude of monopoles restricted to the cortical surface.

The brain source localization defined in section 2 can then be reformulated as a cosparse analysis model fitting problem given by:

$$\begin{cases} \boldsymbol{\Omega}\, \boldsymbol{v} = \boldsymbol{z} \\ \boldsymbol{x} = \boldsymbol{M}\, \boldsymbol{v} \end{cases} \quad (3)$$

where the analysis operator $\boldsymbol{\Omega}$ is given by $\boldsymbol{\Omega} = \boldsymbol{B}^{-1}\boldsymbol{A}$ and the matrix $\boldsymbol{M}$ is a $(N \times L - 1)$ row-reduced identity matrix.

4. THE CoRE ALGORITHM

The purpose of this section is to show how the cosparse analysis model fitting problem presented in section 3 can be solved, giving birth to the CoRE algorithm. First, we reformulate the cosparse analysis model fitting problem (3) as the following convex problem:

$$\underset{\boldsymbol{v}}{\text{minimize}} \ ||\boldsymbol{\Omega}_1\, \boldsymbol{v}||_1 + \lambda ||\boldsymbol{\Omega}_2\, \boldsymbol{v}||_2^2 \quad (4)$$

$$\text{subject to } \boldsymbol{M}\, \boldsymbol{v} = \boldsymbol{x}.$$

where $\boldsymbol{\Omega}_1$ is the $(Q \times L - 1)$ submatrix of $\boldsymbol{\Omega}$ obtained by extracting the rows of $\boldsymbol{\Omega}$ corresponding to the support set $\mathcal{S}$, whereas $\boldsymbol{\Omega}_2$ corresponds to the rows indicated by the complementary set $\bar{\mathcal{S}}$. By choosing the appropriate weight λ, the cosparse solution of the optimization problem (4) will fulfill the assumptions (**A1**) to (**A5**). Namely, $||\boldsymbol{\Omega}_1\, \boldsymbol{v}||_1$ will promote sparsity at the surface of the cortex, while $\lambda ||\boldsymbol{\Omega}_2\, \boldsymbol{v}||_2^2$ will attenuate the signal in the other regions. The linear constraints $\boldsymbol{M}\, \boldsymbol{v} = \boldsymbol{x}$ assure that the model fits the electrode measurements. Depending on the resolution of the cubic grid tuned by L, the problem can reach considerably large scale. Therefore, we propose an efficient first order method in order to solve it, through the Alternating Directions Method of Multiplier (ADMM) framework [12].

First, we reformulate the problem (4) as follows:

$$\underset{\boldsymbol{v}, \boldsymbol{z}_1, \boldsymbol{z_2}}{\text{minimize}} \ ||\boldsymbol{z}_1||_1 + \lambda ||\boldsymbol{z}_2||_2^2 + f(\boldsymbol{v}) \quad (5)$$

$$\text{subject to } \begin{bmatrix} \boldsymbol{\Omega}_1 \\ \boldsymbol{\Omega}_2 \end{bmatrix} \boldsymbol{v} = \begin{bmatrix} \boldsymbol{z}_1 \\ \boldsymbol{z}_2 \end{bmatrix}$$

where f denotes an indicator function of the set $\mathcal{C} = \{\boldsymbol{v} \in \mathbb{R}^{L-1} \mid \boldsymbol{M}\, \boldsymbol{v} = \boldsymbol{x}\}$ given by $f(\boldsymbol{v}) = 0$ for $\boldsymbol{v} \in \mathcal{C}$ and $f(\boldsymbol{v}) = +\infty$ otherwise. Then, the augmented Lagrangian has the following form:

$$L_{\rho_1, \rho_2}(\boldsymbol{v}, \boldsymbol{z}_1, \boldsymbol{z}_2, \boldsymbol{\mu}_1, \boldsymbol{\mu}_2) = ||\boldsymbol{z}_1||_1 + \lambda ||\boldsymbol{z}_2||_2^2 + f(\boldsymbol{v})$$
$$+ \boldsymbol{\mu}_1^{\mathsf{T}} (\boldsymbol{\Omega}_1 \boldsymbol{v} - \boldsymbol{z}_1) + \frac{\rho_1}{2} ||\boldsymbol{\Omega}_1 \boldsymbol{v} - \boldsymbol{z}_1||_2^2$$
$$+ \boldsymbol{\mu}_2^{\mathsf{T}} (\boldsymbol{\Omega}_2 \boldsymbol{v} - \boldsymbol{z}_2) + \frac{\rho_2}{2} ||\boldsymbol{\Omega}_2 \boldsymbol{v} - \boldsymbol{z}_2||_2^2, \quad (6)$$

or after substitution $\boldsymbol{u}_1 = \frac{1}{\rho_1}\boldsymbol{\mu}_1$ and $\boldsymbol{u}_2 = \frac{1}{\rho_2}\boldsymbol{\mu}_2$, the following convenient *scaled form*:

$$L_{\rho_1, \rho_2}(\boldsymbol{v}, \boldsymbol{z}_1, \boldsymbol{z}_2, \boldsymbol{u}_1, \boldsymbol{u}_2) = ||\boldsymbol{z}_1||_1 + \lambda ||\boldsymbol{z}_2||_2^2 + f(\boldsymbol{v})$$
$$+ \frac{\rho_1}{2} ||\boldsymbol{\Omega}_1 \boldsymbol{v} - \boldsymbol{z}_1 + \boldsymbol{u}_1||_2^2 - \frac{\rho_1}{2} ||\boldsymbol{u}_1||_2^2$$
$$+ \frac{\rho_2}{2} ||\boldsymbol{\Omega}_2 \boldsymbol{v} - \boldsymbol{z}_2 + \boldsymbol{u}_2||_2^2 - \frac{\rho_2}{2} ||\boldsymbol{u}_2||_2^2. \quad (7)$$

We now perform an iterative alternating minimization with respect to each of the primal variables $\boldsymbol{v}$, $\boldsymbol{z}_1$ and $\boldsymbol{z}_2$. The minimization with respect to $\boldsymbol{v}$ requires to solve an equality constrained least squares problem:

$$\boldsymbol{v}^{(k+1)} = \underset{\boldsymbol{v}}{\arg \min} \ L_{\rho_1, \rho_2}(\boldsymbol{v}, \boldsymbol{z}_1^{(k)}, \boldsymbol{z}_2^{(k)}, \boldsymbol{u}_1^{(k)}, \boldsymbol{u}_2^{(k)}) =$$
$$\underset{\boldsymbol{v}}{\arg \min} \ ||\boldsymbol{H}\boldsymbol{v} - \boldsymbol{w}||_2^2 \text{ subject to } \boldsymbol{M}\, \boldsymbol{v} = \boldsymbol{x}. \quad (8)$$

where $\boldsymbol{H} = [\sqrt{\rho_1}\, \boldsymbol{\Omega}_1^{\mathsf{T}}, \sqrt{\rho_2}\, \boldsymbol{\Omega}_2^{\mathsf{T}}]^{\mathsf{T}}$ and $\boldsymbol{w} = [\sqrt{\rho_1}\, (\boldsymbol{z}_1^{(k)} - \boldsymbol{u}_1^{(k)})^{\mathsf{T}}, \sqrt{\rho_2}\, (\boldsymbol{z}_2^{(k)} - \boldsymbol{u}_2^{(k)})^{\mathsf{T}}]^{\mathsf{T}}$. Here $\boldsymbol{v}^{(k)}$, $\boldsymbol{z}_1^{(k)}$, $\boldsymbol{z}_2^{(k)}$, $\boldsymbol{u}_1^{(k)}$ and $\boldsymbol{u}_2^{(k)}$ stand for the estimates of the solutions minimizing (7), computed at iteration k. Solving the problem (8) is straightforward when the solution is expressed as the following sum [13, section 16.2]:

$$\boldsymbol{v}^{(k+1)} = \boldsymbol{v}_{\text{p}} + \boldsymbol{K}\boldsymbol{v}_{\text{Null}} \quad (9)$$

where $\boldsymbol{v}_{\text{p}}$ is a particular solution of the underdetermined constraint system $\boldsymbol{M}\, \boldsymbol{v} = \boldsymbol{x}$ and $\boldsymbol{v}_{\text{Null}}$ is the null space component with $\boldsymbol{K}$ a null space basis of $\boldsymbol{M}$. Due to the particular structure of $\boldsymbol{M}$, which is a row-reduced identity matrix, the particular solution is simplified to $\boldsymbol{v}_{\text{p}} = \boldsymbol{M}^{\mathsf{T}} \boldsymbol{x}$ and the columns of $\boldsymbol{K}$ can be simply computed by transposing the rows of the $(L - 1 \times L - 1)$ identity matrix, which do not appear in $\boldsymbol{M}$. Then, by variable substitution in the objective, we obtain:

$$\boldsymbol{v}_{\text{Null}} = \underset{\boldsymbol{y}}{\arg \min} \ ||\boldsymbol{H}\, \boldsymbol{K}\, \boldsymbol{y} + \boldsymbol{H}\, \boldsymbol{M}^{\mathsf{T}} \boldsymbol{x} - \boldsymbol{w}||_2^2. \quad (10)$$

Updating the $\boldsymbol{z}_1^{(k)}$ variable is equivalent to computing the proximity operator for the ℓ_1-norm [14]:

$$\boldsymbol{z}_1^{(k+1)} = \underset{\dot{\boldsymbol{z}}}{\arg \min} \ L_{\rho_1, \rho_2}(\boldsymbol{v}^{(k+1)}, \boldsymbol{z}_1, \boldsymbol{z}_2^{(k)}, \boldsymbol{u}_1^{(k)}, \boldsymbol{u}_2^{(k)})$$
$$= \underset{\dot{\boldsymbol{z}}}{\arg \min} \ ||\boldsymbol{z}_1||_1 + \frac{\rho_1}{2} ||\boldsymbol{z}_1 - \boldsymbol{\Omega}_1 \boldsymbol{v}^{(k+1)} - \boldsymbol{u}_1^{(k)}||_2^2$$
$$\boldsymbol{z}_1^{(k+1)} = \text{prox}_{\frac{1}{\rho_1}\ell_1} \left(\boldsymbol{\Omega}_1 \boldsymbol{v}^{(k+1)} + \boldsymbol{u}_1^{(k)} \right), \quad (11)$$

which is an element-wise soft thresholding (see [12, section 4.4.3] for more details).

The third update concerns the minimization of a weighted sum of two quadratic functionals:

$$
\begin{aligned}
\boldsymbol{z}_2^{(k+1)} &= \underset{\boldsymbol{z}_2}{\arg\min}\, L_{\rho_1,\rho_2}(\boldsymbol{v}^{(k+1)}, \boldsymbol{z}_1^{(k+1)}, \boldsymbol{z}_2, \boldsymbol{u}_1^{(k)}, \boldsymbol{u}_2^{(k)}) \\
&= \underset{\boldsymbol{z}_2}{\arg\min}\, \lambda \|\boldsymbol{z}_2\|_2^2 + \frac{\rho_2}{2}\|\boldsymbol{z}_2 - \boldsymbol{\Omega}_2\boldsymbol{v}^{(k+1)} - \boldsymbol{u}_2^{(k)}\|_2^2 \\
\boldsymbol{z}_2^{(k+1)} &= \frac{\rho_2}{(2\lambda + \rho_2)}\left(\boldsymbol{\Omega}_2\boldsymbol{v}^{(k+1)} + \boldsymbol{u}_2^{(k)}\right). \tag{12}
\end{aligned}
$$

The dual variables are updated in the final stage using the following rules:

$$
\begin{aligned}
\boldsymbol{u}_1^{(k+1)} &= \boldsymbol{u}_1^{(k)} + \boldsymbol{\Omega}_1\boldsymbol{v}^{(k+1)} - \boldsymbol{z}_1^{(k+1)} \\
\boldsymbol{u}_2^{(k+1)} &= \boldsymbol{u}_2^{(k)} + \boldsymbol{\Omega}_2\boldsymbol{v}^{(k+1)} - \boldsymbol{z}_2^{(k+1)} \tag{13}
\end{aligned}
$$

This is the standard way to compute the updates for the scaled Lagrangian multipliers (check [12, section 3.1.1]).

The stopping criterion is based on the primal and dual residuals:

$$
\begin{aligned}
\boldsymbol{r}_{\mathrm{pri}}^{(k+1)} &= \begin{bmatrix}\boldsymbol{\Omega}_1 \\ \boldsymbol{\Omega}_2\end{bmatrix}\boldsymbol{v}^{(k+1)} - \begin{bmatrix}\boldsymbol{z}_1^{(k+1)} - \boldsymbol{u}_1^{(k+1)} \\ \boldsymbol{z}_2^{(k+1)} - \boldsymbol{u}_2^{(k+1)}\end{bmatrix} \\
\boldsymbol{r}_{\mathrm{dual}}^{(k+1)} &= \begin{bmatrix}\rho_1\boldsymbol{\Omega}_1^{\mathsf{T}}\left(\boldsymbol{z}_1^{(k+1)} - \boldsymbol{z}_1^{(k)}\right) \\ \rho_2\boldsymbol{\Omega}_2^{\mathsf{T}}\left(\boldsymbol{z}_2^{(k+1)} - \boldsymbol{z}_2^{(k)}\right)\end{bmatrix}, \tag{14}
\end{aligned}
$$

with appropriate thresholds:

$$
\begin{aligned}
\epsilon_{\mathrm{pri}}^{(k+1)} &= \\
&\sqrt{Q}\epsilon_{\mathrm{A}} + \epsilon_{\mathrm{R}}\max\{\|\boldsymbol{\Omega}\,\boldsymbol{v}^{(k+1)}\|, \|\boldsymbol{z}_1^{(k+1)}\| + \|\boldsymbol{z}_2^{(k+1)}\|\} \\
\epsilon_{\mathrm{dual}}^{(k+1)} &= \\
&\sqrt{L-1}\epsilon_{\mathrm{A}} + \epsilon_{\mathrm{R}}(\|\rho_1\,\boldsymbol{\Omega}_1^{\mathsf{T}}\boldsymbol{u}_1^{(k+1)}\|_2 + \|\rho_2\,\boldsymbol{\Omega}_2^{\mathsf{T}}\boldsymbol{u}_2^{(k+1)}\|_2). \tag{15}
\end{aligned}
$$

where ϵ_{A} and ϵ_{R} denote the absolute and relative tolerances, which we empirically set to 10^{-4} and 10^{-3}, respectively. The iterative procedure terminates when the inequalities $\|\boldsymbol{r}_{\mathrm{pri}}^{(k+1)}\|_2 < \epsilon_{\mathrm{pri}}^{(k+1)}$ and $\|\boldsymbol{r}_{\mathrm{dual}}^{(k+1)}\|_2 < \epsilon_{\mathrm{dual}}^{(k+1)}$ are satisfied.

Regarding the choice of the step sizes ρ_1 and ρ_2, even though the ADMM theory ensures convergence for arbitrary positive values, it is well known that the speed of convergence will be influenced by this choice. Thus, we found a crude heuristics ($\rho_1 = \|\boldsymbol{\Omega}_1\|_2$ and $\rho_2 = \sqrt{\lambda}\|\boldsymbol{\Omega}_2\|_2$) under which the computational time is well-balanced for the wide range of weights λ. Note that the classical matrix norm $\|\cdot\|_2$ subordinate to the corresponding vector norm is usually estimated and then it does not involve heavy computations.

In addition, one can argue that the most expensive step of CoRE algorithm is solving the unconstrained problem (10). However, exact solution of this subproblem is not necessary to obtain the final estimate, hence this step can be efficiently executed by several runs of some appropriate iterative solver (*e.g.* conjugate gradient). Moreover, these can usually be warm-started, which is exactly the way we implemented the minimization (using $\boldsymbol{v}_{\mathrm{Null}}$ computed in the previous iteration as a starting point). It is also important to note that all matrix operators involved are extremely sparse with respect to their dimensions (the numerical density grows only linearly with the dimensions), which is an important advantage of the cosparse approach applied in this context [15].

5. SIMULATIONS

In this section, the numerical performance of the CoRE algorithm is studied on simulated epileptic interictal data and compared with that of the MCE [5], RapMUSIC [6] and 4-D-MUSIC techniques [7].

5.1. Experiments and performance criterion

Two scenarios were considered for this comparison of performance. The first one aimed at studying the influence of the SNR for $N = 128$ electrodes while the second one allowed us to analyse the influence of the number of electrodes for an SNR value of -6 dB.

For both scenarios, $P = 3$ synchronous epileptic dipoles were arranged in $\mathcal{S}$: $P = 3$ monopoles were placed at $\boldsymbol{\theta}_1^- = [1.84, 0.92, 6.44]^{\mathsf{T}}$, $\boldsymbol{\theta}_2^- = [-1.84, -1.84, 6.44]^{\mathsf{T}}$ and $\boldsymbol{\theta}_3^- = [1.84, 5.52, 3.68]^{\mathsf{T}}$, respectively, while the associated monopoles were placed at $\boldsymbol{\theta}_1^+ = [0.92, 0.92, 4.6]^{\mathsf{T}}$, $\boldsymbol{\theta}_2^+ = [-1.84, -1.84, 4.6]^{\mathsf{T}}$ and $\boldsymbol{\theta}_3^+ = [1.84, 4.6, 2.76]^{\mathsf{T}}$, respectively (locations are given in centimeters). Note that the origin (O) of the head model was defined as the intersection of the O-Cz axis (z-axis), the O-T4 axis (x-axis) and the O-Fpz axis (y-axis). A physiologically-relevant model [16] was used to generate the epileptic activity. It is noteworthy that this activity was the same for the three epileptic dipoles, leading to synchronous epileptic sources. On the other hand, the background activity, i.e. the activity of non-epileptic dipoles of $\mathcal{S}$, was generated as Gaussian and as temporally and spatially white. Its power was controlled by a multiplicative coefficient in order to get different SNR values.

As far as the head model is concerned, we used three nested concentric spheres with radius (cm) equal to $7, 8, 9.2$ and conductivities (siemens/cm) equal to $1, 0.0667, 1, 10^{-10}$. One hundred twenty eight electrodes were placed on the scalp sphere using the 10-5 system [17]. The 10-5 system[1] is a logical extension of the 10-20 and 10-10 systems, enabling the use of up to 345 electrodes locations. In addition, in order to apply the FDM and compute the analysis operator $\boldsymbol{A}$, we created a cubic grid with a 0.92 cm spacing ($L^3 = 9261$). Consequently, the size of $\boldsymbol{A}$ and the number Q of dipoles of $\mathcal{S}$ were (4168×4168) and 626, respectively.

---

[1]It is called the 5% system or the 10-5 system because it uses proportional distances of 5% of the total length along contours between skull landmarks, compared to the 20 and 10% distances used in the the 10-20 and 10-10 systems, respectively.
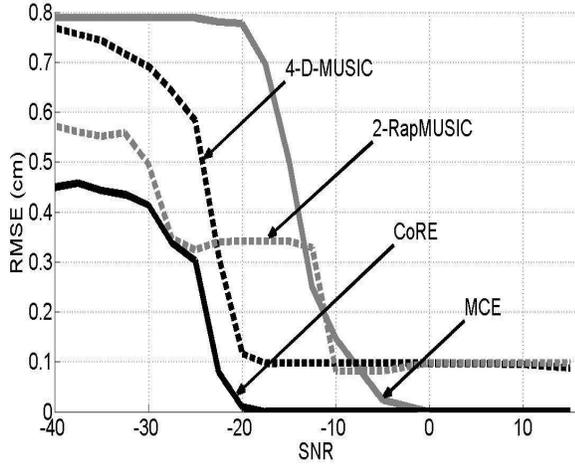
Fig. 1. Behavior of CoRE, MCE, RapMUSIC and 4-D-MUSIC as a function of the SNR for $P = 3$ epileptic dipoles and $N = 128$ electrodes.

Fig. 2. Behavior of CoRE, MCE, RapMUSIC and 4-D-MUSIC as a function of the number of electrodes for $P = 3$ epileptic dipole and an SNR value of -6 dB.

The quality of the source localization was quantified for each method by means of the average Root Mean Square Error (RMSE), which is defined by:

$$RMSE = \frac{1}{PR} \sum_{p=1}^{P} \sum_{r=1}^{R} \left(\min_{1 \leq j \leq P} \left\{ \left\| \boldsymbol{\theta}_p^{(-)} - \widehat{\boldsymbol{\theta}}_j(r) \right\| \right\} \right) \quad (16)$$

where R is the number of realizations fixed to 100, where $\boldsymbol{\theta}_p(r) = [\boldsymbol{\theta}_p^{(-)}(r), \boldsymbol{\theta}_p^{(+)}(r)]$ is the position of the p-th epileptic dipole and where $\widehat{\boldsymbol{\theta}}_j(r) = [\widehat{\boldsymbol{\theta}}_j^{(-)}(r), \widehat{\boldsymbol{\theta}}_j^{(+)}(r)]$ is the j-th dipole location estimated during the r-th Monte Carlo realization. It is noteworthy that from one realization to another, the temporal dynamics of the Q dipoles of $\mathcal{S}$ were changed while the location of the three epileptic dipoles stayed unchanged.

5.2. Computer results

Figure 1 shows the RMSE criterion at the output of the four algorithms as a function of the SNR. It appears that the CoRE method is more robust with respect to the presence of noise than MCE. CoRE succeeds in localizing perfectly the three epileptic dipoles beyond -17.5 dB while the synthesis-based method does not manage to do it below 0 dB. In such a context of synchronous sources, both MUSIC-like approaches do not succeed in localizing the three epileptic dipoles whatever the SNR value is.

Figure 2 displays the RMSE criterion at the output of the four algorithms as a function of the number N of electrodes for an SNR value of -6 dB. CoRE requires at least 64 electrodes to achieve a perfect result for such an SNR value while the other algorithms do not manage to perfectly localize the three synchronous epileptic dipoles whatever the number of electrodes is.
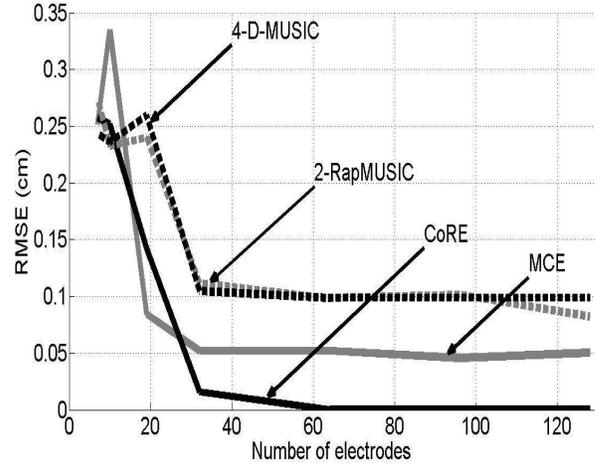
6. CONCLUSION

We proposed a brain source localization method, named CoRE, which uses a physics-driven structured cosparse representation of EEG signals. Our computer results on epileptic interictal data generated using a spherical head model and a physiologically-relevant source model showed the feasability of CoRE approach and its ability to deal with synchronous dipole activities, overcoming RapMUSIC and 4-D-MUSIC in such a context. We also illustrated the better behavior of CoRE for low SNR values compared to the synthesis-based MCE technique. Forthcoming work will include an evaluation of our method on data simulated using a realistic head model but also on real data. Moreover, we will test other optimization strategies to take into account the physiological constraints on current sources.

Appendix

Using Witwer's FDM [11], the total current flow value, $\mathcal{I}_{\ell_1,\ell_2,\ell_3}^{[k]}$, at voxel (ℓ_1, ℓ_2, ℓ_3) and at time kT_e, where T_e the sample period, is given by:

$$\begin{aligned}
\mathcal{I}_{\ell_1,\ell_2,\ell_3}^{[k]} = \mathcal{B}_{\ell_1,\ell_2,\ell_3} \mathcal{V}_{\ell_1,\ell_2,\ell_3}^{[k]} - \\
\mathcal{A}_{\ell_1,\ell_2,\ell_3}^{(1,0,0)} \mathcal{V}_{\ell_1+1,\ell_2,\ell_3}^{[k]} - \mathcal{A}_{\ell_1,\ell_2,\ell_3}^{(-1,0,0)} \mathcal{V}_{\ell_1-1,\ell_2,\ell_3}^{[k]} - \\
\mathcal{A}_{\ell_1,\ell_2,\ell_3}^{(0,1,0)} \mathcal{V}_{\ell_1,\ell_2+1,\ell_3}^{[k]} - \mathcal{A}_{\ell_1,\ell_2,\ell_3}^{(0,-1,0)} \mathcal{V}_{\ell_1,\ell_2-1,\ell_3}^{[k]} - \\
\mathcal{A}_{\ell_1,\ell_2,\ell_3}^{(0,0,1)} \mathcal{V}_{\ell_1,\ell_2,\ell_3+1}^{[k]} - \mathcal{A}_{\ell_1,\ell_2,\ell_3}^{(0,0,-1)} \mathcal{V}_{\ell_1,\ell_2,\ell_3-1}^{[k]}
\end{aligned} \quad (17)$$

with:

$$\begin{aligned}
\mathcal{A}_{\ell_1,\ell_2,\ell_3}^{(m_1,m_2,m_3)} = \\
\frac{2h\sigma(h[\ell_1, \ell_2, \ell_3]^{\mathsf{T}})\sigma(h[\ell_1+m_1, \ell_2+m_2, \ell_3+m_3]^{\mathsf{T}})}{\sigma(h[\ell_1, \ell_2, \ell_3]^{\mathsf{T}}) + \sigma(h[\ell_1+m_1, \ell_2+m_2, \ell_3+m_3]^{\mathsf{T}})}
\end{aligned}$$

$$\mathcal{B}_{\ell_1,\ell_2,\ell_3} = \mathcal{A}_{\ell_1,\ell_2,\ell_3}^{(1,0,0)} + \mathcal{A}_{\ell_1,\ell_2,\ell_3}^{(-1,0,0)} + \mathcal{A}_{\ell_1,\ell_2,\ell_3}^{(0,1,0)} +$$
$$\mathcal{A}_{\ell_1,\ell_2,\ell_3}^{(0,-1,0)} + \mathcal{A}_{\ell_1,\ell_2,\ell_3}^{(0,0,1)} + \mathcal{A}_{\ell_1,\ell_2,\ell_3}^{(0,0,-1)}$$

$$\mathcal{I}_{\ell_1,\ell_2,\ell_3}^{[k]} = \begin{cases} \frac{s(\boldsymbol{\rho},kT_e)}{d} & \text{if } \boldsymbol{\rho}^- = h\,[\ell_1,\ell_2,\ell_3]^{\mathsf{T}} \\ \frac{-s(\boldsymbol{\rho},kT_e)}{d} & \text{if } \boldsymbol{\rho}^+ = h\,[\ell_1,\ell_2,\ell_3]^{\mathsf{T}} \\ 0 & \text{otherwise} \end{cases}$$

where $\mathcal{V}_{\ell_1,\ell_2,\ell_3}^{[k]}$ stands for $v(h[\ell_1,\ell_2,\ell_3]^{\mathsf{T}}, kT_e)$. Note that considering $\boldsymbol{\mathcal{V}} = (\mathcal{V}_{\ell_1,\ell_2,\ell_3}^{[k]})$ as a fourth order array, $\boldsymbol{\mathcal{A}} = (\mathcal{A}_{\ell_1,\ell_2,\ell_3}^{(m_1,m_2,m_3)})$ and $\boldsymbol{\mathcal{B}} = (\mathcal{B}_{\ell_1,\ell_2,\ell_3})$ as third order arrays, and the Hadamard product between multi-way arrays, it is easy to implement the left hand side of equation (17) using matrix programming languages such as Matlab.

7. REFERENCES

[1] R. GRECH, T. CASSAR, J. MUSCAT, K. P. CAMIL-LERI, S. G FABRI, M. ZERVAKIS, P. XANTHOPOU-LOS, V. SAKKALIS, and B. VANRUMSTE, "Review on solving the inverse problem in EEG source analysis," *Journal of NeuroEngineering and Rehabilitation*, vol. 7, pp. 5–25, November 2008.

[2] F. VATTA, F. MENEGHINI, F. ESPOSITO, S. MININEL, and F. DI SALLE, "Realistic and spherical head modeling for EEG forward problem solution: A comparative cortex-based analysis," *Computational Intelligence and Neuroscience*, Article ID 972060, 2010.

[3] T. PIOTROWSKI, D. GUTIERREZ, I. YAMADA, and J. ZYGIEREWICZ, "Reduced-rank neural activity index for eeg/meg multi-source localization," in *ICASSP'14, IEEE International Conference on Acoustics Speech and Signal Processing*, Florence, Italy, May 4-9 2014.

[4] R. O. SCHMIDT, "Multiple emitter location and signal parameter estimation," *IEEE Transactions On Antennas Propagation*, vol. 34, no. 3, pp. 276–280, Mar. 1986, Reprint of the original 1979 paper from the RADC Spectrum Estimation Workshop.

[5] K. UUTELA, M. HAMALAINEN, and E. SOMER-SALO, "Visualization of magnetoencephalographic data using minimum current estimates," *Elsevier NeuroImage*, vol. 10, no. 2, pp. 173–180, August 1999.

[6] J. C. MOSHER and R. M. LEAHY, "Source localization using Recursively Applied and Projected (RAP) music," *IEEE Transactions On Signal Processing*, vol. 47, no. 2, pp. 332–340, Feb. 1999.

[7] L. ALBERA, A. FERREOL, D. COSANDIER-RIMELE, I. MERLET, and F. WENDLING, "Brain source localization using a fourth-order deflation scheme," *IEEE Transactions Biomedical Engineering*, vol. 55, no. 2, pp. 490–501, Feb. 2008.

[8] A. GRAMFORT, D. STROHMEIER, HAUEISEN, HAMALAINEN, and M. KOWALSKI, "Time-frequency mixed-norm estimates: Sparse m/eeg imaging with non-stationary source activations," *Elsevier NeuroImage*, vol. 70, pp. 410–422, April 2013.

[9] S. NAM, M. E. DAVIES, M. ELAD, and R. GRIBON-VAL, "The cosparse analysis model and algorithms," *Applied and Computational Harmonic Analysis*, vol. 34, no. 1, pp. 30–56, January 2013.

[10] M. MOHR and B. VANRUMSTE, "Comparing iterative solvers for linear systems associated with the finite difference discretisation of the forward problem in electro-encephalographic source analysis," *Medical and Biological Engineering and Computing*, vol. 41, pp. 75–84, 2003.

[11] J. G. WITWER, G. J. TREZEK, and D. L. JEWETT, "The effect of media inhomogeneities upon intracranial electrical fields," *IEEE Transactions on Biomedical Engineering*, vol. 19, no. 5, pp. 352–362, 1972.

[12] S. BOYD, N. PARIKH, E. CHU, B. PELEATO, and J. ECKSTEIN, "Distributed optimization and statistical learning via the alternating direction method of multipliers," *Foundations and Trends in Machine Learning*, vol. 3, no. 1, pp. 1–122, 2011.

[13] S. J. WRIGHT and J. NOCEDAL, *Numerical optimization*, vol. 2, Springer New York, 1999.

[14] F. BACH, R. JENATTON, J. MAIRAL, and G. OBOZINSKI, "Convex optimization with sparsity-inducing norms," *Optimization for Machine Learning*, pp. 19–53, 2011.

[15] S. KITIC, N. BERTIN, and R. GRIBONVAL, "Review of cosparse signal recovery methods applied to sound source localization," in *GRETSI 13, XXIVeme colloque sur le Traitement du Signal et des Images*, Brest, France, September 3-6 2013.

[16] B. H. JANSEN and V. G. RIT, "Electroencephalogram and visual evoked potential generation in a mathematical model of coupled cortical columns?," *Biological Cybernetics*, vol. 73, no. 4, pp. 357–366, Sept. 1995.

[17] R. OOSTENVELDA and P. PRAAMSTRA, "The five percent electrode system for high-resolution EEG and ERP measurements," *Clinical Neurophysiology, Elsevier*, vol. 112, no. 4, pp. 713–719, April 2001.